ROYAL SOCIETY OF CHEMISTRY

PAPER

Check for updates

A porous Brønsted superacid as an efficient and durable solid catalyst†

Qi Sun,‡*[a] Kewei Hu,‡[a] Kunyue Leng,[b] Xianfeng Yi,[c] Briana Aguila, [ID][d] Yinyong Sun, [ID][c] Anmin Zheng, [ID][c] Xiangju Meng,[a] Shengqian Ma[d] and Feng-Shou Xiao [ID]‡*[a]

The development of catalysts able to assist industrial chemical transformations is a topic of high importance. In view of the versatile catalytic capabilities of acid catalysts, extensive research efforts are being made to develop porous superacid materials with a high density of accessible active sites to replace molecular acid catalysts. Herein, we report the rational development of a porous Brønsted superacid by combining important elements that target high strength acidity into one material, as demonstrated by grafting the sulfonic acid group onto a highly fluorinated porous framework, where the acid strength and stability are greatly enhanced by an electron-withdrawing environment provided by the polymer backbone, reminiscent of that seen in Nafion® resin. In addition, the densely arranged acid groups that are confined in the three-dimensional nanospace facilitate the transfer of hydrons, thereby further increasing the acidity. By virtue of the pore structure and strong acidity, this system exhibits excellent performance for a wide range of reactions, far outperforming commercial acid resins under repeated batch and flow reaction conditions. Our findings demonstrate how this synthetic approach may instruct the future design of heterogeneous acid catalysts with advantageous reaction capabilities and stability.

Introduction

The development of porous materials offers great improvements in catalyst design for efficient large-scale chemical processes.[1–6] In particular, solid acid catalysts,[7–12] as represented by zeolites, have played an indispensable role in the petroleum refinery industry for continuous throughput and efficient separation.[13,14] Yet, due to the lack of high performance solid acid catalysts, a significant number of acid-catalyzed reactions still mainly rely on molecular acids.[15,16] Transferring the high activity of these catalysts into their solid states remains challenging because the low grafting degree of acid groups and the rigidity of solid supports prevent them from cooperating in the transfer of protons, an essential feature in the manifestation of

superacidity.[17] In addition, the lack of suitable porous materials with unique properties to compensate such an inevitable loss after immobilization leads to the acidity of the resultant solids being much weaker than their liquid structural analogues. Therefore, the development of nanostructured strongly acidic catalysts, particularly those with superacidity (acids stronger than 100% sulfuric acid), is still in the portfolio of researchers and such materials will pave the way toward alleviating the various existing burdens imposed by current synthetic technologies pertaining to the environment and the overall cost.[18,19]

To tackle the challenges of designing high performance acid materials and especially those with the superacidic character, we were inspired by perfluororesinsulfonic acids, such as Nafion®,[20] well-known superacid catalysts, and numerous developed elegant systems on the journey to achieve efficient porous acid catalysts.[21–28] From the established knowledge that the strength of acidity is primarily determined by the nature of the acid group (*e.g.* –SO$_3$H > –COOH), the electronic properties of the backbone and the density of acid groups in the materials, wherein reducing the distance strengthens the acidity by enhancing their cooperation, it is believable that combining all these essential elements into one material may give rise to a superior catalyst. We thus postulate that if the sulfonic acid groups can be grafted onto a highly fluorinated porous framework with a preset position for modification, a catalyst with a high density yet readily accessible acid sites that are arranged

[a]Key Lab of Applied Chemistry of Zhejiang Province, Department of Chemistry, Zhejiang University, Hangzhou 310028, China. E-mail: sunqichs@zju.edu.cn; fsxiao@zju.edu.cn

[b]School of Chemical Engineering and Technology, Harbin Institute of Technology, Harbin 150001, China

[c]State Key Laboratory of Magnetic Resonance and Atomic and Molecular Physics, Wuhan Institute of Physics and Mathematics, Chinese Academy of Sciences, Wuhan 430071, China
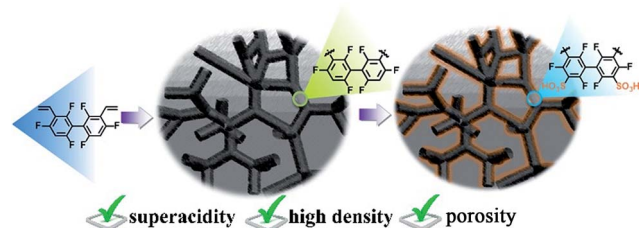
[d]Department of Chemistry, University of South Florida, 4202 E. Fowler Avenue, Tampa, Florida 33620, USA

in electron-withdrawing three-dimensional nanospaces will be achieved. The strong electronegativity of the fluorine atoms not only makes the molecule less susceptible to chemical and electrophilic attack, but also stabilizes the sulfonic acid anions and thereby facilitates the leaving of the protons on them. This is anticipated to afford new acid materials with fast reaction kinetics and high acid strength, in conjugation with great stabilities, which surmount the prime issues of low efficiency encountered by Nafion® as a result of the low surface area and low density of acid groups,[29] as well as the low acid strength of many other solid catalysts.[30] To fulfill these tasks, porous organic polymers (POPs)[31–33] showing great promise as versatile candidates for acid catalysis were used. Due to their amenable synthesis, high surface areas, and exceptional chemical stability, they have emerged as one of the prime alternatives to traditional porous materials, such as active carbon and silica gels, with great potential to address the ongoing energy and environmental challenges.[34–40] In this contribution, we demonstrate that the sulfonic acid groups grafted on a highly fluorinated porous polymer framework act as a catalyst in a range of industrially important transformations with a combination of high activity and selectivity that are superior to those of all benchmark heterogeneous acid catalysts tested.

In developing versatile POP-based acid catalysts, we sought to employ $2,2',4,4',6,6'$-hexafluorobiphenyl as a building block given that it is highly fluorinated yet molecularly designable. The modulation property of this compound ensures its feasibility to be constructed into a highly porous framework and to be endowed with abundant active sites. Moreover, the performance of the acid groups, in turn, could benefit from the electron-withdrawing polymer backbone (Scheme 1). In view of materials synthesis for practical applications, free-radical induced polymerization of vinyl-functionalized monomers is particularly attractive with these considerations: in addition to the excellent monomer tolerance and cost-effective synthesis, the adapted polymerization conditions allow adjustment of the pore structure and introduce hierarchical porosity for the enhancement of mass transfer.[41,42] We thus surmised that modifying sulfonic acid moieties onto such a framework could serve as a means to obtain a very efficient solid catalyst for a wide range of acid catalyses. Indeed, in liquid phase processes, the resultant catalyst with higher intrinsic acidity exhibits outstanding properties that are many times better than those of the sulfonic acid groups grafted on an analogous nonfluorinated porous polymer and commercial acid resins, as

well as approaching or exceeding those observed for H_2SO_4 as a catalyst. Most notably, this catalyst, with its hierarchical porosity, is highly active and durable under fixed bed conditions, allowing for the elimination of solvent and easy separation of the reaction products, thereby holding great promise to replace the existing technologies.

Materials and methods

Materials

Commercially available reagents were purchased in high purity and used without purification. Solvents were purified according to standard laboratory methods. THF and DMF were distilled over $LiAlH_4$ and CaH_2, respectively.

Catalyst preparation

Synthesis of the fluorinated porous organic polymer (FPOP). $2,2',4,4',6,6'$-Hexafluoro-3,3′-divinyl-1,1′-biphenyl (1.0 g) was dissolved in THF (10 mL), followed by addition of azobisisobutyronitrile (AIBN, 25 mg). The mixture was transferred into an autoclave at 100 °C for 24 h. The title material was obtained after being washed with CH_2Cl_2 and dried under vacuum.

Synthesis of the sulfonated FPOP (FPOP-SO₃H). Fuming sulfonic acid (20%, 40 mL) was added dropwise to a 100 mL flask containing 500 mg of FPOP. The mixture was stirred at room temperature for 48 h, and then 50 °C for another 48 h, after which the mixture was poured into ice water and washed with an excess of water until the pH of the filtrate reached around 7.

Characterization

The gas adsorption isotherms were collected on a surface area analyzer ASAP 2020. The N_2 sorption isotherms were measured at 77 K using a liquid N_2 bath. Scanning electron microscopy (SEM) images were collected using a Hitachi SU 1510 or Hitachi SU 8000. TGA was carried out on a Q50 thermogravimetric analyzer under a N_2 atmosphere at a heating rate of 10 °C min^{-1}. IR spectra were recorded on a Nicolet Impact 410 FTIR spectrometer. X-ray photoelectron spectroscopy (XPS) spectra were recorded on a Thermo ESCALAB 250 with Al Kα irradiation at $\theta = 90°$ for X-ray sources, and the binding energies were calibrated using the C 1s peak at 284.9 eV. CHNS elemental analyses were performed on a Perkin-Elmer series II CHNS analyzer 2400. Diffuse reflectance ultraviolet-visible (UV-vis) spectra were measured with a PE Lambda 20 spectrometer, and $BaSO_4$ was used as an internal standard sample. ^1H NMR spectra were recorded on a Bruker Avance-400 (400 MHz) spectrometer. Chemical shifts are expressed in ppm downfield from TMS at $\delta = 0$ ppm, and J values are given in Hz. ^{13}C (125 MHz) cross-polarization magic-angle spinning (CP-MAS), and ^{19}F (470 MHz) MAS solid-state NMR experiments were performed on a Bruker Avance-500 spectrometer. Before the ^{31}P MAS NMR measurements, the samples were placed in a Pyrex cell equipped with a stopcock. The sample cell was outgassed at 120 °C. A CH_2Cl_2 solution containing a known amount of TMPO (100%, Alfa) was added under an inert atmosphere to prevent

Scheme 1 Synthetic illustration of the fluorinated porous organic polymer (FPOP) and its subsequent sulfonation with oleum.

This journal is © The Royal Society of Chemistry 2018

J. Mater. Chem. A, 2018, **6**, 18712–18719 | **18713**

moisture absorption. After being homogeneously mixed, CH_2Cl_2 solvent was removed by evacuation at room temperature and then transferred into a NMR sample rotor. $(NH_4)_2HPO_4$ was chosen as a reference with the ^{31}P chemical shift at 1.0 ppm.

Results and discussion

Synthesis of the fluorinated porous organic polymer (FPOP) framework

In our attempts to target a sulfonic acid grafted fluorinated porous framework, a two-step synthesis was employed due to the incompatibility of the highly active vinyl groups under the harsh conditions of the sulfonation process. The fluorinated porous organic polymer (FPOP) framework can be quantitatively obtained by polymerization of the vinyl-functionalized hexafluorobiphenyl under solvothermal conditions in tetrahydrofuran (THF) at 100 °C for 24 h with the assistance of azobisisobutyronitrile (AIBN), where the monomer was readily synthesized from 1,3,5-trifluorobenzene, as detailed in the ESI.†

Structural characterization of the fluorinated porous organic polymer framework (FPOP)

The chemical composition and structure of the FPOP were determined by solid-state ^{13}C and ^{19}F NMR spectroscopy. The ^{13}C MAS NMR spectrum of the FPOP showed a characteristic signal centered at 31.2 ppm, which is assignable to the opened double bonds formed after polymerization.[43] The chemical shifts at 102.6, 116.0, and 160.2 ppm can be attributed to the nonsubstituted, substituted, and adjacent aromatic carbons to the F atoms in the polymer backbone, respectively, which are in accord with those of the monomer (Fig. S1, ESI†). The ^{19}F MAS NMR spectrum of the FPOP gave a clear F signal, however, due to the chemical anisotropy of solid samples, the well-separated ^{19}F signals in the range of −110.6 to −109.3 ppm of liquid NMR of the monomer appeared as a broad signal at −111.6 ppm in solid NMR of the resultant polymer (Fig. S2, ESI†). These results indicate that the hexafluorobiphenyl moieties are maintained during the polymerization process. The morphology of the FPOP was examined by scanning electron microscopy (SEM) and transmission electron microscopy (TEM), showing that the FPOP displayed a rough surface that is composed of randomly agglomerated small particles with sizes ranging from several nanometers to over tens of nanometers, giving rise to interconnected meso- and macroporous objects (Fig. 1a and b). To investigate the details of the pore characteristics of the FPOP, N_2 sorption isotherms at 77 K were measured. The adsorption curve exhibited a sharp uptake of N_2 at low relative pressure ($P/P_0 < 0.1$) and a hysteresis loop at higher relative pressure ($0.4 < P/P_0 < 0.95$), manifesting the hierarchically porous structure of the FPOP[44] and the Brunauer–Emmett–Teller (BET) surface area was calculated to be 866 m^2 g^{-1} (Fig. 1c).

Introduction of sulfonic acid groups into the fluorinated porous organic polymer (FPOP-SO₃H) framework

With a porous and fluorinated framework available, we proceeded to introduce sulfonic acid groups. By treatment of the
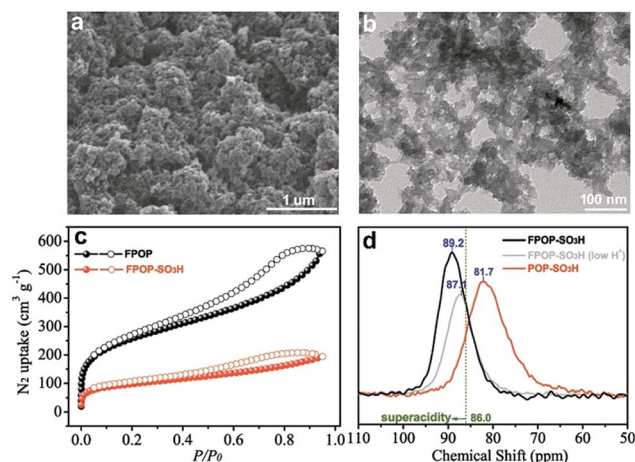

Fig. 1 Porous structure and acid strength characterization. (a) SEM and (b) TEM of the FPOP, (c) N_2 sorption isotherms collected at 77 K, and (d) ^{31}P MAS NMR spectra of TMPO chemically adsorbed on the FPOP-SO₃H and POP-SO₃H, respectively.

FPOP with oleum at room temperature for 48 h and then 50 °C for another 48 h, a sulfonated solid was obtained, denoted as the FPOP-SO₃H. The successful sulfonation of FPOP was confirmed by X-ray photoelectron spectroscopy (XPS), FT-IR, solid-state ^{13}C NMR studies, and elemental analysis. The appearance of the sulfur signal at a binding energy of 169.1 eV in the XPS spectrum of the FPOP-SO₃H suggests the existence of sulfonic acid groups (Fig. S3, ESI†).[45] In addition, the emergence of the characteristic bands of S=O at 1079 cm^{-1} and 1197 cm^{-1} compared with those of the pristine FPOP[45] verifies the presence of sulfonic acid groups (Fig. S4, ESI†). The high throughput of the sulfonation process was determined by the significantly weakened peak assigned to the nonsubstituted aromatic carbons at around 102.6 ppm and the concomitant emergence of a peak at 129.4 ppm ascribed to the aromatic carbon substituted by the –SO₃H group in the ^{13}C MAS NMR spectrum of the FPOP-SO₃H (Fig. S5, ESI†). The retention of F species of the FPOP during the sulfonation process was indicated by the high intensity of F signals in the XPS and ^{19}F MAS NMR spectra of the FPOP-SO₃H (Fig. S3 and S5, ESI†). The slight shift of F signals in the FPOP-SO₃H compared with those in the FPOP can be a result of the introduction of electron-withdrawing sulfonic acid groups, which lead to the benzene ring becoming more negative thus decreasing the electron density of F species. The acid content of the FPOP-SO₃H was measured by ion exchange with NaCl, followed by titration of the free H^+ with NaOH, showing that it contains 3.56 mmol g^{-1} of accessible H^+ sites (Table S1, ESI†). To validate the titration results, elemental analysis was performed. Based on the S element content, the sulfonic acid group amount in the FPOP-SO₃H was calculated to be 3.49 mmol g^{-1}, which is consistent with that from the titration experiments. SEM and TEM images of the FPOP-SO₃H displayed similar morphologies to the FPOP, indicative of its structural integrity and retention of the hierarchical pore structure after sulfonation (Fig. S6, ESI†). N_2 sorption results revealed that the BET surface area of the FPOP-SO₃H was

18714 | J. Mater. Chem. A, 2018, 6, 18712–18719

This journal is © The Royal Society of Chemistry 2018

340 m^2 g^{-1} with a pore volume of 0.3 cm^3 g^{-1}, confirming its pore structure (Fig. 1c). The decreased surface area can be reasonably attributed to the increased mass after the functionality addition. Based upon the calculations of the nonlocal density functional theory method (NLDFT), it is found that the pore size is distributed in the range of 2.8–18 nm (Fig. S7, ESI†).

Taking a lesson from Nafion®, it is suggested that the presence of electron-withdrawing F atoms in the structure increases significantly both the thermal stability and acid strength of the sulfonic acid groups.[46] To determine the role of fluorine species in the performance of sulfonic acid groups in the FPOP-SO$_3$H, side-by-side comparisons were made with the nonfluorinated analogue, POP-SO$_3$H (BET: 561 m^2 g^{-1}, Fig. S8–S10, ESI†). This material was synthesized by polymerization of 4,4′-divinylbiphenyl and then sulfonated as described above (see details in the ESI†). Titration experiments were carried out to calculate the accessible H$^+$ content in the POP-SO$_3$H, giving as high as 3.84 mmol g^{-1}, indicative of a similar acid content in the POP-SO$_3$H and FPOP-SO$_3$H. To compare the thermal stability of the FPOP-SO$_3$H and POP-SO$_3$H, thermogravimetric analysis (TGA) under a N$_2$ atmosphere was performed and both samples showed a multi-step decomposition pattern (Fig. S11 and S12, ESI†). The first step mass loss before 150 °C is attributed to the removal of adsorbed H$_2$O. A second mass loss is likely associated with desulfonation and the remaining is likely due to the decomposition of the polymer matrix. It is interesting to find that the FPOP-SO$_3$H exhibits higher decomposition temperatures for both the sulfonic groups (290 °C $vs.$ 230 °C) and the polymer framework (430 °C $vs.$ 350 °C) in relation to those of the POP-SO$_3$H, promising for the FPOP-SO$_3$H to have long-term stable performance under high temperature conditions. The increased thermal resistance after introduction of F species could be a result of the hydrogen bonding interactions between H and F species that stabilize the overall structure.[47]

Acidity strength test

To evaluate the acid strength, the Hammett method was employed by using a range of closely related UV-vis probes. Specifically, the Hammett acidity (H_0) was tested by immersing a solid in a specific indicator solution and checking whether the color of the solid changes to that of the acid form of the indicator, or there is a change in the position of the indicator absorption band in the visible spectrum, or the H_0 value of that solid is the same or lower than the pKa of the conjugate acid of the indicator. After being soaked in a benzene solution of 4-nitrofluorobenzene, the FPOP-SO$_3$H displayed a new UV-vis peak at around 460 nm, which is attributed to the acid form of 4-nitrofluorobenzene, indicating $H_0 \leq -12.4$ and placing it in the superacid region ($H_0 \leq -12.0$), while the FPOP-SO$_3$H exhibited moderate acidity ($-4.4 \geq H_0 \geq -8.1$), as evidenced by the fact that it showed a colour change in 2,4-dinitroaniline benzene solution but not in anthraquinone solution.[48] To provide more qualitative information, probe molecule studies were performed. Given the sensitivity and isotropicity of the ^{31}P chemical shift of the probe trimethylphosphine oxide (TMPO) according to its interaction strength with a Brønsted acid site, it

has proven to be an informative tool for identifying the acidity of multiple acid sites.[49,50] The ^{31}P MAS NMR spectrum of TMPO after interaction with the FPOP-SO$_3$H sample shows a singlet peak at 87.1 ppm, appearing to possess an acid strength higher than the threshold of superacidity (86.0 ppm). By contrast, a notable decrease in acid strength was observed for the POP-SO$_3$H catalyst, as revealed by the TMPO resonance upfields to 81.7 ppm, providing a consistent interpretation of the acidity evaluated by Hammett analysis. These results were further validated by their performance in catalytic α-pinene isomerization (Scheme S1, ESI†), where the FPOP-SO$_3$H showed appreciable conversion of α-pinene with low camphene yield and high secondary reactions of limonene, while the POP-SO$_3$H afforded inferior conversion and relatively high selectivity towards camphene and limonene (Fig. S13, ESI†).[51] It is worth mentioning that the FPOP with a low degree of sulfonation (2.04 mmol g^{-1}) gave an adsorbed TMPO ^{31}P NMR signal at 87.1 ppm. Together, these results indicate that both F species and the amount of sulfonic acid groups introduced play critical roles in the acidity of the resultant materials. In the acid-catalyzed conversions, carbocationic mechanisms are generally accepted. The strong acidity facilitates the generation of carbocations which may also result in the formation of coke. However, improved diffusion by introduction of pore structures in the solid acid catalysts has proven to be an effective way to inhibit such a side reaction and thereby the overall efficiency.[12]

Catalytic evaluation

To demonstrate the usefulness and effectiveness of the FPOP-SO$_3$H, the esterification of palmitic acid with ethanol was used as a test platform to compare its catalytic performance against that of the POP-SO$_3$H, and two benchmark solid acid catalysts Amberlyst-15 and Nafion® NR50, as well as a mineral acid, H$_2$SO$_4$. This particular reaction was chosen because esterification of higher fatty acids has spurred a great deal of interest, due to the potential utilization of the product as a biofuel. Also, the reaction is especially important in the synthesis of biodiesel from low-cost feedstocks containing a large amount of free fatty acids, as such compounds must undergo acid-catalyzed esterification before transesterification of the larger triglycerides being carried out using a base.[52] Fig. 2a shows the time course
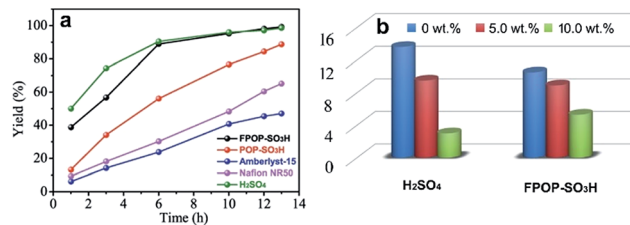

Fig. 2 Catalytic kinetics and water resistance tests. (a) Ethyl palmitate yield $versus$ time plots over various catalysts. Reaction conditions: palmitic acid (2.0 mmol), ethanol (2.0 mL), catalyst (0.04 mmol accessible H$^+$, 2.0 mol%), and 60 °C. (b) Water sensitivity of palmitic acid esterification catalyzed by H$_2$SO$_4$ and the FPOP-SO$_3$H. Reaction conditions: palmitic acid (10.0 mmol), ethanol (10.0 mL), catalyst (0.04 mmol accessible H$^+$), 60 °C, and in the presence of various amounts of water.

of ethyl palmitate formation over various catalytic systems with a catalyst loading level of 2.0 mol% accessible H^+ sites relative to palmitic acid (Table S2, ESI†). The initial turnover frequencies (TOF) from this figure are 9.4 h^{-1} for the FPOP-SO$_3$H, 3.3 h^{-1} for the POP-SO$_3$H, 1.5 h^{-1} for Amberlyst-15, and 2.3 h^{-1} for Nafion® NR50, indicating that the TOF of the FPOP-SO$_3$H is at least four and six times higher than those of Nafion® NR50 and Amberlyst-15 catalysts, respectively, in the initial 1 h. In addition, the reaction using the FPOP-SO$_3$H approaches a full conversion after 13 h, while at that time, the POP-SO$_3$H, Amberlyst-15, and Nafion® NR50 only gave the product yields of 88.7%, 47.0%, and 65.1%, respectively. The catalytic tests section in the ESI† has the TOF formula and a detailed procedure on calculating yields from GC. Considering the same amount of active sites employed, the much higher activity observed for the FPOP-SO$_3$H relative to other solid catalysts tested should be attributed to the combined contributions from its high acidity and accessibility of active sites. In comparison with H$_2$SO$_4$, the FPOP-SO$_3$H exhibited an inferior initial activity, giving a TOF value by a factor of 1.3 lower than that of H$_2$SO$_4$ in the beginning 1 h (9.4 h^{-1} *vs.* 12.5 h^{-1}). However, their discrepancy in kinetics became smaller along with the reaction. Specifically, the FPOP-SO$_3$H reached around 90% and 95% product yields within 6 h and 10 h, respectively, and it also took the same time for H$_2$SO$_4$ to accomplish such conversions. We assumed that this phenomenon should result from their different level of tolerance towards water. As an esterification byproduct, water was found to significantly inhibit H$_2$SO$_4$ involved catalysis.[52] To prove this hypothesis, their resistance against water poisoning was evaluated. The effect of water on the FPOP-SO$_3$H- and H$_2$SO$_4$-catalyzed esterification was studied using initial reaction kinetics (<15% conversion) with varying amounts of initially added water. This permits a better determination of the effect of water on the catalyst, because the rate is little affected by the reverse reaction when only small amounts of the ester products are present. In Fig. 2b, the water sensitivities of the FPOP-SO$_3$H and H$_2$SO$_4$ are compared. The catalytic activity of H$_2$SO$_4$ was significantly inhibited with increasing water concentration in the reaction mixture. After 1 h of reaction, the system with 10 wt% initial water content had a conversion around 80% lower than that with no initial water added (13.6% *vs.* 3.0%). By contrast, the FPOP-SO$_3$H exhibited less deactivation by water than H$_2$SO$_4$, as demonstrated by less drop in activity (10.5% *vs.* 5.3%). After proving the water resistance, we assessed the heterogeneity of the FPOP-SO$_3$H under reaction conditions by evaluating the possible leaching of acid species. To this end, the filtrate obtained by catalyst recovery after 3 h was allowed to react continuously. Negligible ester formation was observed, providing evidence against leaching of a soluble active catalyst (Fig. S14, ESI†). Furthermore, the retention of reactivity upon recycling reaffirms that the material is stable under the catalytic conditions. The above results underscore the advantages of the FPOP-SO$_3$H as an environmentally friendly solid acid catalyst (Fig. S15, ESI†). To verify the structural stability of the catalyst during the reaction, we carried out the N$_2$ sorption tests. It was revealed that negligible changes were observed in terms of both surface area and pore volume (Fig. S16, ESI†).
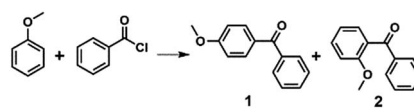
To further demonstrate the versatility of the FPOP-SO$_3$H towards other acid catalyzed reactions we have studied its performance in Friedel–Crafts alkylation and acylation reactions which are one of the top research priorities in industry and academia.[53-55] The traditional catalysts used in acylation chemistry suffer from several drawbacks from the use of stoichiometric amounts of catalysts (AlCl$_3$ and BF$_3$) to extensive problems with the disposal of the associated waste stream, motivating more direct and atom-economical procedures employing a catalytic amount of activator. Using acylation of anisole with benzoyl chloride as a model reaction, once again, the FPOP-SO$_3$H is the most active material, giving rise to a 95.3% benzoyl chloride conversion within 10 h. Even more interesting was the finding that the desired (4-methoxyphenyl)(phenyl)methanone (1) was the only product observed (Table 1, entry 1). By contrast, other catalysts, Amberlyst-15, Nafion® NR50, the POP-SO$_3$H, and H$_2$SO$_4$ were found to be much less effective, affording the conversion of benzoyl chloride at 44.8%, 61.3%, 55.3%, and 39.3%, respectively, under identical conditions. In addition, being different from the FPOP-SO$_3$H, both the *para* and *ortho* acylated products, whose ratios were in the range of 1.66 to 4.68, were detected for the other catalytic systems studied (Table 1, entries 2–5). The observed unique catalytic performance of the FPOP-SO$_3$H should be a result of the combination of strong acidity and unique pore structure.

Similarly, in the Friedel–Crafts alkylations between benzyl alcohol and toluene, FPOP-SO$_3$H also exhibited the most satisfactory results compared with other catalysts tested by taking into account both activity and selectivity. In this reaction, along with the formation of the desired benzylation product (monobenzylated aromatic), dehydrative coupling of benzyl alcohol usually occurs to yield dibenzyl ether.[56] As shown in Table S2 (ESI†), the FPOP-SO$_3$H exhibited a full benzyl alcohol conversion after 6 h with a satisfyingly preferred product yield rivaling with that of Nafion® NR50 (76.8% *vs.* 83.4%), but far surpassing it in terms of kinetics. In contrast, the benzylation product/ether selectivity of Amberlyst-15 and Nafion® NR50 was in the

Table 1 Catalytic data in the Friedel–Crafts acylation of benzoyl chloride and anisole over various catalysts[a]

Entry	Catalyst	Conv. (%)	Sel. (%)	
			1	**2**
1	FPOP-SO$_3$H	95.3	>99.5	n.d.[b]
2	POP-SO$_3$H	55.3	82.4	17.6
3	Amberlyst-15	44.8	78.2	21.8
4	Nafion® NR50	61.3	79.6	20.4
5	H$_2$SO$_4$	39.3	62.4	37.6

[a] Reaction conditions: benzoyl chloride (2.0 mmol), anisole (1.0 g), 100 °C, 10 h, and catalyst (0.04 mmol accessible H^+). [b] Not detectable.

18716 | *J. Mater. Chem. A*, 2018, **6**, 18712–18719

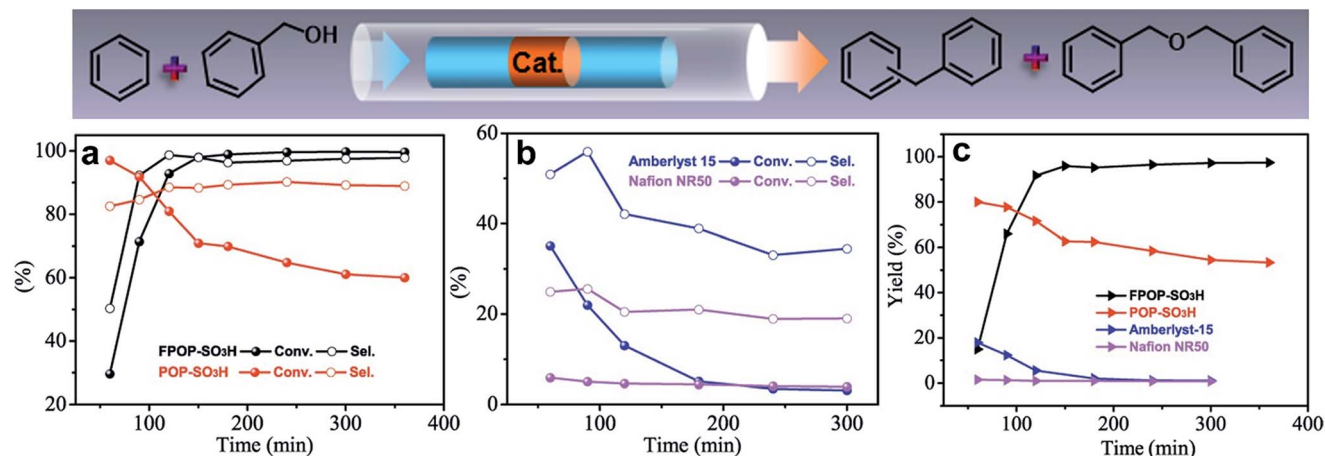This journal is © The Royal Society of Chemistry 2018

Fig. 3 Fixed-bed reaction evaluation. (a and b) Conversion of benzyl alcohol and selectivity of diphenylmethane and (c) plots of diphenylmethane yields *versus* time over various catalysts (50 mg of FPOP-SO$_3$H, POP-SO$_3$H, Amberlyst-15, or 300 mg of Nafion® NR50) in the benzylation reaction of benzene with benzyl alcohol. Reaction conditions are detailed in the catalytic tests in the ESI.†

range of 1.6–1.9 and H$_2$SO$_4$ only gave a ratio of around 1 : 1. These results suggest that the FPOP-SO$_3$H constitutes a competitive alternative to replace some traditional homogeneous catalysts.

The fast reaction rate combined with the stability and recyclability (Tables S3 and S4, ESI†) of the FPOP-SO$_3$H prompted us to evaluate its performance under continuous fixed-bed reaction conditions to reduce the footprint of chemical plants and increase their productivity, modularity, and flexibility. To highlight the superiority of the FPOP-SO$_3$H, the performances of other heterogeneous catalytic systems were compared, taking the benzylation reaction of benzene with benzyl alcohol as an example. Fig. 3a and b show the profile of reaction conversion and selectivity as a function of time over the FPOP-SO$_3$H, POP-SO$_3$H, Amberlyst-15, and Nafion® NR50. The FPOP-SO$_3$H showed a remarkable increase in catalytic activity in the initial stage, approaching a full conversion after 150 min (this delay is likely because when the instrument is initially started it requires time to stabilize, Fig. S17, ESI†). Impressively, the activity and selectivity toward the target product diphenylmethane remained essentially constant after that; this is in striking contrast to the POP-SO$_3$H, which gave rise to a steady decrease in conversion from 97% to 60% and consistent selectivity at around 90% during the reaction time. Under identical conditions, the two nonporous resin catalysts, Amberlyst-15 and Nafion® NR50, exhibited very low conversion and selectivity and even worse, the performance is not stable, as demonstrated by the fact that the conversion of the reaction underwent a sharp decrease and both of the catalysts gave less than 5% conversion after 180 min. These results thereby underscore the importance of the introduction of hierarchical porosity for the maintenance of the catalyst's high performance over extended reaction times by improving the accessibility of reactants to catalytic sites and providing faster transport paths for the removal of products and byproducts. In addition to this, the presence of F species also plays an essential role in maintaining the long-term stability of active sites. To further assess

the productivity of the catalysts, the yield according to the conversion and selectivity was calculated. The FPOP-SO$_3$H exhibited a yield that increased with reaction time and reached a stable value of about 97% after 150 min. In contrast, a steady decrease in yield over the reaction time was observed for all of the other catalysts tested. Specifically, in terms of the amount of product after the reaction time period of 120 min, the FPOP-SO$_3$H far exceeded all of the other catalysts, producing 1.83, 91.3, and 131.7 times as much product as that by the POP-SO$_3$H, Amberlyst-15, and Nafion® NR50, respectively at 300 min. It is worth mentioning that due to the hierarchical porosity of the FPOP-SO$_3$H, diffusion is not a rate determining step given the fact that we increased the reactant benzoyl alcohol injection rate from 0.06 mL min^{-1} to 0.07 mL min^{-1} and performed the catalytic evaluations under otherwise identical conditions. A benzoyl alcohol conversion of 93% was achieved within 60 min (Fig. S17, ESI†). The synergistic effects of high acidity and hierarchical porosity provide the FPOP-SO$_3$H with the highest performance values known among porous-material-based solid acid catalysts, placing it within striking distance of the all-time benzylation record and thereby presenting a new benchmark for acid materials.[57–62]

Conclusions

In summary, a hierarchically porous superacid material with a high surface area and abundant accessible active sites was synthesized by grafting sulfonic acid groups onto a highly fluorinated porous polymer framework. The resultant material has a much higher surface area and accessible H$^+$ content than the benchmark superacid Nafion® NR50, acting as a remarkable solid acid catalyst with superior long-term stability in a range of industrially important and molecular catalyst-dominated reactions. The improved catalytic performances are attributed to the combined contribution of the faster transport paths of reagents to active sites resulting from the porous structure, and increased acid strength and stability of

This journal is © The Royal Society of Chemistry 2018

J. Mater. Chem. A, 2018, **6**, 18712–18719 | **18717**

sulfonic acid groups grafted on a highly fluorinated framework. We believe that these features will profoundly advance the application and fabrication of solid superacid catalysts. In light of the excellent catalytic performance, porous fluorosulfonic acids, as presented here, might be promising alternatives to replace hazardous and corrosive homogeneous acid catalysts, thus making a major contribution to green chemistry.

Conflicts of interest

There are no conflicts to declare.

Acknowledgements

References

1 M. E. Davis, *Nature*, 2002, **417**, 813–821.

2 A. G. Slater and A. I. Cooper, *Science*, 2015, **348**, 988.

3 R. Rinaldi and F. Schüth, *Energy Environ. Sci.*, 2009, **2**, 610–626.

4 J. Liu, L. Chen, H. Cui, J. Zhang, L. Zhang and C.-Y. Su, *Chem. Soc. Rev.*, 2014, **43**, 6011–6061.

5 Y. Zhang and S. N. Riduan, *Chem. Soc. Rev.*, 2012, **41**, 2083–2094.

6 D. S. Su, S. Perathoner and G. Centi, *Chem. Rev.*, 2013, **113**, 5782–5816.

7 X. Zhang, Y. Zhao, S. Xu, Y. Yang, J. Liu, Y. Wei and Q. Yang, *Nat. Commun.*, 2014, **5**, 3170.

8 K. Nakajima and M. Hara, *ACS Catal.*, 2012, **2**, 1296–1304.

9 T. M. Jyothi, M. L. Kaliya and M. V. Landau, *Angew. Chem., Int. Ed.*, 2001, **40**, 2881–2884.

10 M. A. Harmer and Q. Sun, *Appl. Catal., A*, 2001, **221**, 45–62.

11 X. Wang, R. Liu, M. M. Waje, Z. Chen, Y. Yan, K. N. Bozhilov and P. Feng, *Chem. Mater.*, 2007, **19**, 2395–2397.

12 F. Liu, K. Huang, A. Zheng, F.-S. Xiao and S. Dai, *ACS Catal.*, 2018, **8**, 372–391.

13 A. Corma, *Chem. Rev.*, 1997, **97**, 2373–2420.

14 X. Meng and F.-S. Xiao, *Chem. Rev.*, 2014, **114**, 1521–1543.

15 T. Okuhara, *Chem. Rev.*, 2002, **102**, 3641–3666.

16 K. Tanabe and W. F. Hölderich, *Appl. Catal., A*, 1999, **181**, 399–434.

17 D. Fărcaşiu, A. Ghenciu, G. Marino and K. D. Rose, *J. Am. Chem. Soc.*, 1997, **119**, 11826–11831.

18 T. Xu, N. Kob, R. S. Drago, J. B. Nicholas and J. F. Haw, *J. Am. Chem. Soc.*, 1997, **119**, 12231–12239.

19 K. Ishihara, A. Hasegawa and H. Yamanoto, *Angew. Chem., Int. Ed.*, 2001, **40**, 4077–4079.

20 F. J. Waller and R. W. Van Scoyoc, *CHEMTECH*, 1987, **17**, 438.

21 Y. Xu, W. Gu and D. Gin, *J. Am. Chem. Soc.*, 2004, **126**, 1616–1617.

22 J. H. Clark, *Acc. Chem. Res.*, 2002, **35**, 791–797.

23 D. J. Macquarrie, S. J. Tavener and M. A. Harmer, *Chem. Commun.*, 2005, 2363–2365.

24 B. Török, I. Kiricsi, Á. Molnár and G. A. Olah, *J. Catal.*, 2000, **193**, 132–138.

25 F. Zhang, C. Liang, X. Wu and H. Li, *Angew. Chem., Int. Ed.*, 2014, **53**, 8498–8502.

26 R. Alamillo, A. J. Crisci, J. M. R. Gallo, S. L. Scott and J. A. Dumesic, *Angew. Chem., Int. Ed.*, 2013, **52**, 10349–10541.

27 C. Tian, C. Bao, A. Binder, Z. Zhu, B. Hu, Y. Guo, B. Zhao and S. Dai, *Chem. Commun.*, 2013, **49**, 8668–8670.

28 F. Liu, L. Wang, Q. Sun, L. Zhu, X. Meng and F.-S. Xiao, *J. Am. Chem. Soc.*, 2012, **134**, 16948–16950.

29 M. A. Harmer, W. E. Farneth and Q. Sun, *J. Am. Chem. Soc.*, 1996, **118**, 7708–7715.

30 A. Pourjavadi, S. H. Hosseini, M. Doulabi, S. M. Fakoorpoor and F. Seidi, *ACS Catal.*, 2012, **2**, 1259–1266.

31 Y. Xu, S. Jin, H. Xu, A. Nagai and D. Jiang, *Chem. Soc. Rev.*, 2013, **42**, 8012–8031.

32 L.-B. Sun, X.-Q. Liu and H.-C. Zhou, *Chem. Soc. Rev.*, 2015, **44**, 5092–5147.

33 T. Ben, C. Pei, D. Zhang, J. Xu, F. Deng, X. Jing and S. Qiu, *Energy Environ. Sci.*, 2011, **4**, 3991–3999.

34 B. Li, Y. Zhang, D. Ma, Z. Shi and S. Ma, *Nat. Commun.*, 2014, **5**, 5537.

35 G. Ji, Z. Yang, H. Zhang, Y. Zhao, B. Yu, Z. Ma and Z. Liu, *Angew. Chem., Int. Ed.*, 2016, **55**, 9685–9689.

36 Q. Zhao, P. Zhang, M. Antonietti and J. Yuan, *J. Am. Chem. Soc.*, 2012, **134**, 11852–11855.

37 S. Fischer, J. Schmidt, P. Strauch and A. Thomas, *Angew. Chem., Int. Ed.*, 2013, **52**, 12174–12178.

38 X. Ding and B.-H. Han, *Angew. Chem., Int. Ed.*, 2015, **54**, 6536–6639.

39 Y. Xie, T.-T. Wang, X.-H. Liu, K. Zou and W.-Q. Deng, *Nat. Commun.*, 2013, **4**, 1960.

40 C. Yang, B. C. Ma, L. Zhang, S. Lin, S. Ghasimi, K. Landfester, K. A. I. Zhang and X. Wang, *Angew. Chem., Int. Ed.*, 2016, **55**, 9202–9206.

41 Y. Yue, R. T. Mayes, J. Kim, P. F. Fulvio, X.-G. Sun, C. Tsouris, J. Chen, S. Brown and S. Dai, *Angew. Chem., Int. Ed.*, 2013, **52**, 13458–13462.

42 Q. Sun, Z. Dai, X. Liu, N. Sheng, F. Deng, X. Meng and F.-S. Xiao, *J. Am. Chem. Soc.*, 2015, **137**, 5204–5209.

43 Q. Sun, M. Jiang, Z. Shen, Y. Jin, S. Pan, L. Wang, X. Meng, W. Chen, Y. Ding, J. Li and F.-S. Xiao, *Chem. Commun.*, 2014, **50**, 11844–11847.

44 Q. Sun, S. Ma, Z. Dai, X. Meng and F.-S. Xiao, *J. Mater. Chem. A*, 2015, **3**, 23871–23875.

45 F. Liu, W. Kong, C. Qi, L. Zhu and F.-S. Xiao, *ACS Catal.*, 2012, **2**, 565–572.

46 M. Alvaro, A. Corma, D. Das, V. Fornés and H. García, *Chem. Commun.*, 2004, 956–957.

47 H. Lv, X. Zhao, Z. Li, D. Yang, Z. Wang and X. Yang, *Polym. Chem.*, 2014, **5**, 6279–6286.

48 A. Corma, *Chem. Rev.*, 1995, **95**, 559–614.

49 A. Zheng, H. Zhang, X. Lu, S.-B. Liu and F. Deng, *J. Phys. Chem. B*, 2008, **112**, 4496–4505.

50 J. P. Osegovic and R. S. Drago, *J. Catal.*, 1999, **182**, 1–4.

51 R. Rachwalik, Z. Olejniczak, J. Jiao, J. Huang, M. Hunger and B. Sulikowski, *J. Catal.*, 2007, **252**, 161–170.

52 I. K. Mbaraka, D. R. Radu, V. S.-Y. Lin and B. H. Shanks, *J. Catal.*, 2003, **219**, 329–336.

53 Y. Liu, E. Lotero and J. G. Goodwin Jr, *J. Catal.*, 2006, **242**, 278–286.

54 G. A. Olah, *Friedel-Crafts Chemistry*, Wiley-Interscience, New York, 1973.

55 A. E. W. Beers, I. Hoek, T. A. Nijhuis, R. S. Downing, F. Kapteijn and J. A. Moulijn, *Top. Catal.*, 2000, **13**, 275–280.

56 G. Sartori and R. Maggi, *Chem. Rev.*, 2006, **106**, 1077–1104.

57 B. Li, K. Leng, Y. Zhang, J. J. Dynes, J. Wang, Y. Hu, D. Ma, Z. Shi, L. Zhu, D. Zhang, Y. Sun, M. Chrzanowski and S. Ma, *J. Am. Chem. Soc.*, 2015, **137**, 4243–4248.

58 Y. Sun and R. Prins, *Appl. Catal., A*, 2008, **336**, 11–16.

59 K. Na, C. Jo, J. Kim, K. Cho, J. Jung, Y. Seo, R. J. Messinger, B. F. Chmelka and R. Ryoo, *Science*, 2011, **333**, 328–332.

60 P. Horcajada, S. Surblé, C. Serre, D.-Y. Hong, Y.-K. Seo, J.-S. Chang, J.-M. Grenèche, I. Margiolaki and G. Férey, *Chem. Commun.*, 2007, 2820–2822.

61 J. J. Chiu, D. J. Pine, S. T. Bishop and B. F. Chmelka, *J. Catal.*, 2004, **221**, 400–412.

62 J. Dou and H. C. Zeng, *J. Am. Chem. Soc.*, 2012, **134**, 16235–16246.

This journal is © The Royal Society of Chemistry 2018

J. Mater. Chem. A, 2018, **6**, 18712–18719 | **18719**